Resistance Switch in a Minimal-Fullerene Chain in Vertically Stacked Electrodes

Takuma Hirama,[a, b] *Masato Takei,*[a, b] *Hiroyuki Motoyama,*[a, b] *Masafumi Ohta,*[a, b] *Hiroshi Suga,**[a, b] *Takatsugu Wakahara,*[c] *and Kazuhito Tsukagoshi**[, b, a]

[a] Chiba Institute of Technology, Tsudanuma, Narashino, Chiba 275-0016, Japan

[b] Research Center for Materials Nanoarchitectonics (MANA), National Institute for Materials Science (NIMS), Tsukuba, Ibaraki 305-0044, Japan

[c] Electronic Functional Macromolecules Group, Research Center for Macromolecules and Biomaterials, National Institute for Materials Science (NIMS), Tsukuba, Ibaraki 305-0044, Japan

Keywords: Fullerene, polymerization, C_{60} pyrrolidine tris-acid (CPTA), resistance switching, vertically stacked structure, nanochannel, fullerene derivative

ABSTRACT

A switch element with a minimal fullerene chain was prepared by spin coating a C_{60} pyrrolidine trisaccharide (CPTA) film between vertically stacked two metallic electrodes. In this structure, the nanoscale length of the fullerene chain can be adjusted by changing the thickness of the CPTA film by changing spin coating condition. The CPTA film had a rough surface that led to cause distance fluctuations between the two electrodes. At the thinnest point, a nanoscale chain could be selectively formed as a conductive channel that exhibited binary resistance switching between high- and low-resistance states. This resistance change was primarily caused by the polymerization and depolymerization of the nanoscale C_{60} chain in response to external voltage inputs. When the film thickness was reduced to approximately 3.7 nm, corresponding to 3-4 fullerene chains bridging the two electrodes, a stable switching sequence was reproducibly achieved.

INTRODUCTION

The amount of information is expected to increase explosively in the future because of the utilization of big data from artificial intelligence and the Internet of Things. Therefore, highly integrated electronic devices are expected to be developed. Among these devices, the resistive random access memory (ReRAM) is a promising candidate. ReRAM is composed of an oxide layer that is vertically sandwiched between two metal electrodes and has features such as non-volatility and high integration.[1–7] ReRAM is a promising high-density device[8] that has a variable resistance layer with a thickness of 30–50 nm based on the principle of oxygen vacancies.[9] However, further miniaturization has been facing difficulty by fluctuations in the operating voltage during the resistance change transition process because the filaments in the channel layer are randomly formed during the setting process.[10,11] ReRAM has been developed using organic molecules[12–15] to achieve low costs and easy manufacturing, although the operation of these devices is unstable in high temperature and humidity environments. Furthermore, miniaturization and integration are difficult because the organic elements are easily damaged and/or structurally changed in the conventional electron device fabrication process. Soft chemical materials can easily be damaged during the cyclic operation of switching and/or memory functions.

Fullerene devices, which are intermediate materials between inorganic and organic materials, have been developed.[16–19] The individual C_{60} molecule is a rigid spherical shell composed of carbon atoms and can be functionalized similarly to organic

molecules.[20,21] Although fullerene surfaces can be chemically functionalized for various applications, the intrinsic structure of fullerene is stable even in conventional device fabrication processes.[22–24] Fullerene C_{60} can accept up to six electrons into the lowest unoccupied molecular orbital (LUMO) at a low energy level, providing excellent electron acceptor characteristics in n-type semiconductors.[25–27] Furthermore, intermolecular bonds between fullerenes can be connected to form a polymer chain in the film and/or bulk, allowing the electrical function of a device to be controlled by bond connections. Based on these properties, fullerene has been proposed as a material in electrical devices.

Single fullerene devices are expected to find applications in various devices. However, an electrode needs to be developed for the device structure. Fullerene devices require a precise fabrication method to fix a 1 nm fullerene between electrodes, thus functional applications of single-fullerene devices, particularly in integrated circuits, have to overcome concerns of reproducibility issues in device fabrication. Therefore, we developed fullerene devices using a different strategy: bulk and/or film.[16-19]

We have demonstrated the electrical switching behavior of device structures with fullerene crystal wires[16,17] or thin films based on fullerene derivatives.[18,19] Fullerene crystal nanowires fabricated by the liquid-liquid interfacial precipitation (LLIP) method were treated with devices that bridged metal electrodes.[16,17] In particular, we prepared a C_{60} pyrrolidine tris-acid (CPTA) film device by spin coating from a solution. In general, CPTA has been used as an efficient electron transport layer in perovskite solar cells.[28–

[31] An advantage of CPTA is its good solubility in organic solution and uniform thin film coating on the substrate because the carboxylic acid groups in CPTA form interfacial chemical bonds with the oxygen-deficient oxide film on the surface, which solves the problem of agglomeration during film formation.[28,32,33] Furthermore, an amorphous CPTA film having poor conductivity can be locally activated by electron beam (EB) lithography to form conduction channels in devices.[34–38] In our previous report, submicron-scale conductive paths between the pre-patterned metallic electrodes were prepared using EB irradiation of CPTA films. Two-terminal measurements of the activated CPTA films show binary resistance switching in response to external inputs.[18] Very recently, we have fabricated a 10–20 nm prototype device as an ideal resistance switch composed of a narrow, short channel and a C_{60} chain of approximately 20 fullerenes in the nanogap.[19]

In this study, we developed a fullerene switch with nonvolatile memory function using a CPTA thin film sandwiched between two vertically stacked electrodes. The thickness of the CPTA thin film formed by spin coating corresponded to the channel length, which can potentially shrink to the nanoscale level. The thickness of the CPTA thin films was adjusted by varying the spin-coating conditions. We demonstrate a resistance switch in a minimal-fullerene chain using this vertically stacked structure with CPTA. The observed channel length of 3.7 nm corresponded to 3–4 fullerene chains, which is much shorter than that in CPTA nanogap devices[19] where approximately 20 fullerenes form fullerene nanochains. This device had a vertical structure similar to that of ReRAM, thus

this device is expected to be advantageous in future high-density integration applications.

EXPERIMENTAL SECTION

The device structure, with detailed observations, is shown in Figure 1. A vertically stacked fullerene device was fabricated on a silicon substrate with a 250 nm thick oxide film (Figure 1a). A bottom electrode composed of a 10-nm-thick gold palladium (AuPd: Au/Pd = 8/2) film with a 1 μm width was patterned by EB lithography and then deposited by thermal evaporation. The surface of the bottom electrode was coated with a 1-nm-thick layer of InO_x by atomic layer deposition. Thin films of InO_x are highly resistive in in-plane DC resistance measurements and work as adhesion layers to uniformly spin coat the nanoscale-thick CPTA film. Average thickness of CPTA ranged from a few nanometers to tens of nanometers and was reproducibly controlled by the spin-coating condition. A second 10-nm-thick AuPd electrode was deposited on the CPTA film through a metal stencil mask. Even though the thinnest CPTA film was a few nanometers thick, the two-terminal measurement through the film was non-conductive, which was reproducibly obtained in the fabricated devices, indicating that the nanometer-thin CPTA film had no pinhole in the electrode overlapping region (Supporting Information: Figure S1). The dense packing of the CPTA film without pinholes ensured the uniform adhesion of the molecules on the oxide surface. Although the CPTA film is widely used as an electron transport layer in perovskite solar cells,[28–

[30,32] solar cells are centimeter-scale or larger, and the work-function alignment is carefully adjusted at the interface. In our vertically stacked device with only micrometer-scale electrode overlapping, the as-prepared film showed extremely low conduction below the detection limit of the measurement system. To activate the CPTA channel and form a conductive spot area, a 1 μm x 1 μm square region on the bottom electrode was irradiated by EB before the top electrode evaporation.

A large-energy EB current in the EB irradiation (50 keV) of the CPTA film may decompose CPTA into fullerene C_{60}s and chemical functional additives. In addition to the preset EB exposure, high density current flow under a high electric field causes local heating and stimulates decomposition. In a reference experiment using (6,6)-phenyl-C61 butyric acid methyl ester (PCBM), its chemical substituent element was removed at 340 °C to return to the original C_{60}s.[39] After the removal of the functional additive, the C_{60} positions could be rearranged under a high electric field between the narrow nanogaps, allowing denser packing of C_{60}s to increase the current.

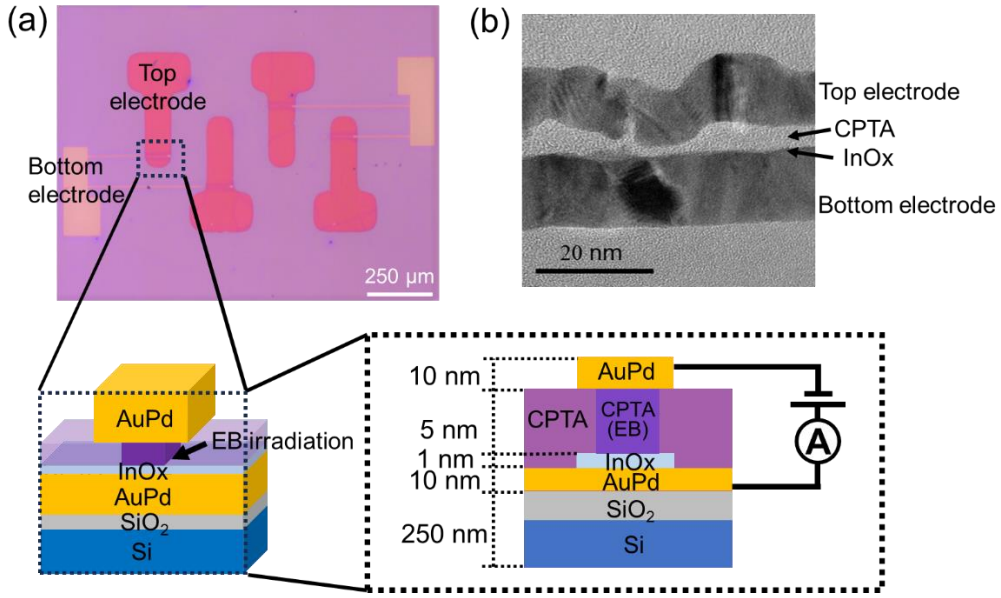

Figure 1. (a) Optical photo image with a schematic diagram of the vertical structural element, (b) Cross-sectional transmission electron microscopy (TEM) image of the vertical structural element. C_{60} pyrrolidine tris-acid (CPTA) was coated at 4000 rpm.

A cross-sectional image of the electrode overlapping the region with the CPTA layer was obtained using transmission electron microscopy (TEM) (Figure 1b). The surface roughness of the bottom electrode was a root mean square roughness (Rms) of 0.13 nm (Figure 2a), and the top electrode was winding with a constant thickness. This image suggests that the spin-coated CPTA film forms a rough surface because of its special volume and partial self-aggregation. In the observed image areas, the thinnest section of the CPTA film was approximately 3.7 nm with an extra roughness of 3 nm. In addition to the TEM cross-sectional observations, atomic force microscopy (AFM) showed morphology of the surface (Figure 2b). The Rms value of the CPTA surface obtained by AFM was 0.90 nm, indicating the CPTA surface was much rougher than the InO_x surface.

Deep hollows in the AFM image were potential electron injection points, which appeared at 3–5 points in every 1 μm square.

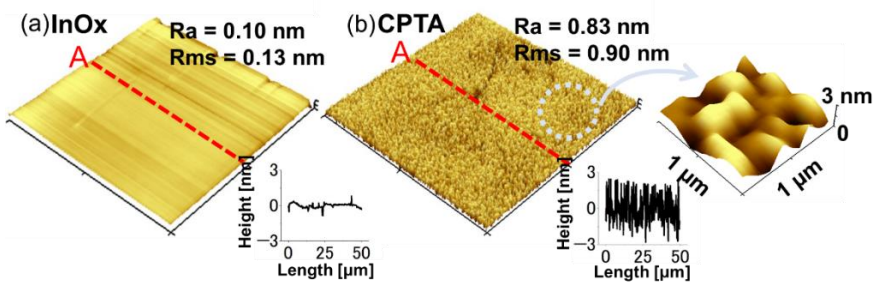

Figure 2. Atomic force microscopy (AFM) morphology image of the electrode surface and C_{60} pyrrolidine tris-acid (CPTA) surface spin coated at 4000 rpm. (a) Surface of the InO_x film on the bottom electrode. (b) CPTA surface. CPTA was spin coated on the surface of InO_x (a). Scanned area of the images was 50 μm square, and the magnified area in (b) was 1 μm square. Each inset of the height profile shows surface roughness at the cutting line marked by A. Abbreviations: Average roughness (Ra) and Root mean square roughness (Rms).

Current-voltage (*I*–*V*) measurements were performed in a CPTA vertically stacked electrode device by applying a DC voltage from the bottom to the top electrode. Measurements were performed at room temperature in an environment of 1.0×10^{-3} Pa or less.

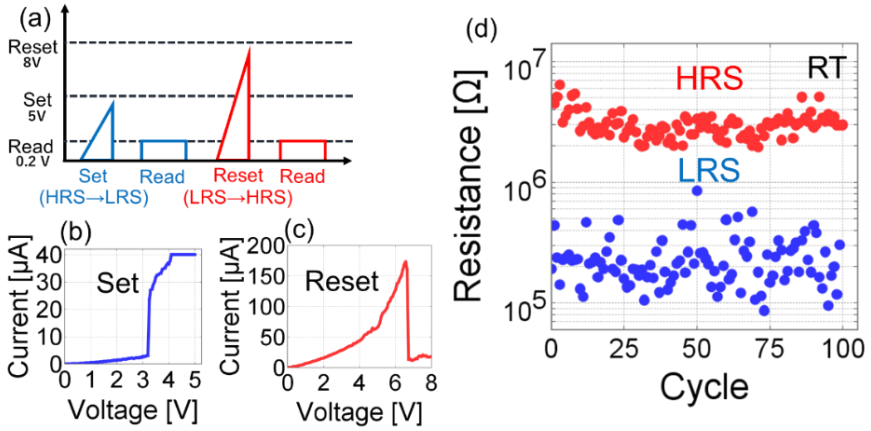

Figure 3. (a) One cycle of the external voltage input sequence for the resistance switching effect in a vertically stacked structure. set voltage changed the system from the HRS to the LRS. reset voltage was for the NDR operation. Read voltage was for reading the voltages of the LRS and HRS. One cycle of the input voltage sequence was 66 sec. (b) set operation *I-V* characteristic as a function of input voltage and reset operation (c). (d) Sequential resistance changes of 100 cycles.

Sequential switching was achieved (Figure 3). For the status-reading operation of the channel, a low voltage (0.2 V) was applied to measure the channel resistance. For set operation to change the device resistance from a high-resistance state (HRS) to a low-resistance state (LRS), a gradual voltage input was applied between the two metallic electrodes (Figure 3a). With a gradual increase in voltage, a small nonlinear current was generated, and the current sharply increased at 3.2 V (Figure 3b). With a sharp increase in current, the set operation generated a C_{60} polymer chain between the two electrodes. In addition, the reset operation was executed by applying a gradual input voltage of 8 V (Figure 3c). Before the voltage reached 8 V, a rapid drop in the current was observed at 6.5 V. This rapid decrease is recognized as the negative differential resistance (NDR) change, indicating the disconnection of the conductive chain of fullerenes between the

two electrodes. At the NDR, the resistance decreased from the LRS to the HRS. If the set operation was applied again to the HRS, the resistance changed to the LRS. Subsequently, the sequential cyclic operation of switching between the LRS and HRS was obtained, as shown in Figure 3(d). Note that no current flowed through the channel between the two electrodes without preset EB exposure; therefore, this switching behavior was not observed (Figure S1). Furthermore, when an inverse polarity in the voltage application was performed, current might flow from top electrode to bottom electrode. This measurement configuration did not show the switching behavior.

The NDR and turn-on characteristics were systematically measured as a function of the CPTA film thickness. Three films of different thicknesses were prepared by changing the spin-coating rotation speed (Table 1), which resulted in a thickness change from 3.7 to 15.3 nm. At these variable spin-speeds, the CPTA solution was fixed: 100 μg of CPTA was dissolved in 10 ml N, N-dimethylformamide (DMF).[18,40] The film thickness was measured at the step edge of the film by AFM with reasonable reproducibility.

Table 1. Thicknesses of the C_{60} pyrrolidine tris-acid (CPTA) films prepared by different spin-coating conditions. The thickness was measured by atomic force microscopy (AFM) at the step of the film edge.

Spin-coating condition [rpm]	Thickness [nm]
4000 (thin)	3.7 ± 0.5
3000 (middle)	7.5 ± 1.9
2000 (thick)	15.3 ± 1.2

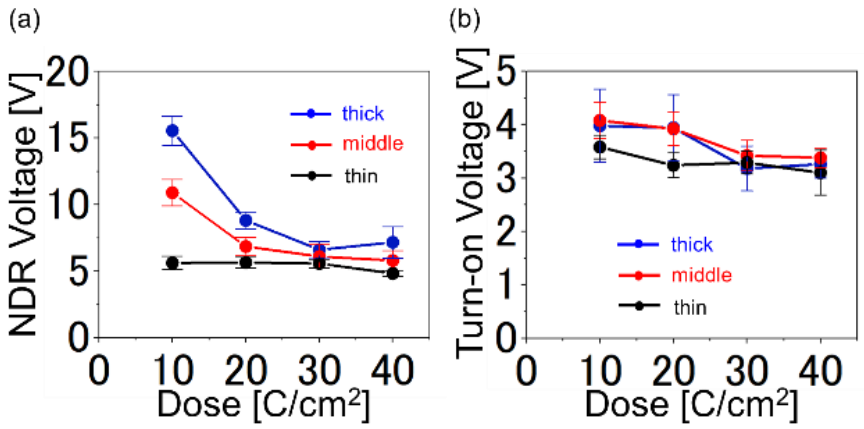

Figure 4. Relationship between the dose of electron beam exposure and voltage for different film thicknesses. Voltage of the negative differential resistance (NDR) transition at the reset voltage (a), and turn-on transition at the set voltage (b). The average voltages of the NDR and turn-on were evaluated for 100 cycles of *I*–*V* measurements.

Using a vertical structure, the film thickness dependence, corresponding to the fullerene chain length dependence, was investigated in terms of the switching characteristics (Figure 4). The average voltages of the NDR observed in the reset operation (Figure 3c) and turn-on in the set operation (Figure 3b) were evaluated in one hundred *I*–*V* measurements, as shown in Figures 4a and 4b. Both voltages were plotted in terms of the EB dose density exposed to the film (Figure S1). The voltage of the NDR transition decreased as the film thickness decreased (Figure 4a). Although the turn-on voltage showed a similar trend to the NDR voltage, the decrease in voltage as a function of decreasing film thickness was less significant (Figure 4b). The difference in these results could be due to different transition mechanisms.[19] The NDR transition relied on the depolymerization of the fullerene polymer chain, which could be caused by the local heating effect in and near the chain channel. Then, current flow through the

thicker film with the larger resistance required a larger voltage to achieve a sufficient temperature for the depolymerization. In contrast, the turn-on transition is caused by a local voltage applied to the locally disconnected section in the fullerene chain. The voltage was always slightly greater than 3 volts in a different device configuration.[19] Although the total remaining section of the continuous fullerene chain might have a larger resistance for the longer chain, the resistance at the disconnected section could be dominant. The thickness dependence of the turn-on voltage hardly changed even when the film thickness changed. Fluctuation distributions of the NDR voltage and turn-on voltage were depicted in Supporting Information (Figure S2).

The dose-density dependence of EB irradiation (Figure 4) on both transition voltages was also plotted. The NDR transition voltage in the thick film exhibited pronounced dose dependence, whereas the thin film showed independence. This dose dependence supports the above discussion on the transition mechanism: a thick film with a large resistive section in the conduction chain could be influenced by electron irradiation forming the polymer connection. The turn-on transition voltage was insensitive to the NDR transition voltage. This also supports the above turn-on repair mechanism in the local disconnected area caused by the applied voltage. Interestingly, the NDR voltage in the thin film was also insensitive to the dose density, indicating that a few minimal fullerene chains in the vertically stacked electrode structure could be dominated by the direct current injection between the electrodes through the 3–4 fullerene space.

CONCLUSIONS

A short nanoscale fullerene chain with a binary resistance switch was fabricated in a vertically stacked two-electrode structure with a fullerene-derivative CPTA layer. The advantage of this scheme is that the thickness of the CPTA channel layer can be reproducibly controlled by changing the spin-coating conditions. Furthermore, self-aggregation of individual CPTA molecules causes the rough surface, resulting in the forming current injection points between the two electrodes. Even when the channel length was narrowed to 3.7 nm, corresponding to 3–4 fullerene chain lengths bridging the two electrodes, a stable switching sequence was reproducibly achieved. A thinner fullerene layer, which is a conductive channel, lowers the operating voltage. The operating voltage was reduced by controlling the amount of electron beam irradiation to promote the polymerization and depolymerization of fullerene polymers. The low voltages, simple device structure, and straightforward method are advantageous for future applications.

ASSOCIATED CONTENT

Supporting Information

The following files are available free of charge.

Additional experimental details and theoretical support on the experimental result (PDF)

Figure S1. Electron beam irradiation effect in the channel layer.

Figure S2. Histogram of transition voltage for variable film thickness.

AUTHOR INFORMATION

Corresponding Authors

Hiroshi Suga – Chiba Institute of Technology, Tsudanuma, Narashino, Chiba 275-0016, Japan; orcid.org/ 0000-0003-4333-4898; Email: hiroshi-suga@it-chiba.ac.jp

Kazuhito Tsukagoshi – Research Center for Materials Nanoarchitectonics (MANA), National Institute for Materials Science, Tsukuba, Ibaraki 305-0044, Japan; orcid.org/0000-0001-9710-2692; Email: TSUKAGOSHI.kazuhito@nims.go.jp

Co-Authors

Takuma Hirama – *Chiba Institute of Technology, Narashino, Chiba 275-0016, Japan; International Center for Materials Nanoarchitectonics (WPI-MANA), National Institute for Materials Science (NIMS), Tsukuba, Ibaraki 305-0044, Japan;* orcid.org/0009-0001-9436-1557

Masato Takei – *Chiba Institute of Technology, Narashino, Chiba 275-0016, Japan; International Center for Materials Nanoarchitectonics (WPI-MANA), National Institute for Materials Science (NIMS), Tsukuba, Ibaraki 305-0044, Japan;* orcid.org/0000-0002-3522-0033

Hiroyuki Motoyama – *Chiba Institute of Technology, Narashino, Chiba 275-0016,*

Japan; International Center for Materials Nanoarchitectonics (WPI-MANA), National Institute for Materials Science (NIMS), Tsukuba, Ibaraki 305-0044, Japan; orcid.org/0009-0003-1390-9053

Masafumi Ohta – *Chiba Institute of Technology, Narashino, Chiba 275-0016, Japan; International Center for Materials Nanoarchitectonics (WPI-MANA), National Institute for Materials Science (NIMS), Tsukuba, Ibaraki 305-0044, Japan;* orcid.org/0009-0006-6883-2358

Takatsugu Wakahara – *Electronic Functional Macromolecules Group, Research Center for Macromolecules and Biomaterials, National Institute for Materials Science (NIMS), Tsukuba, Ibaraki 305-0044, Japan;* orcid.org/0000-0002-6365-3215

Author Contributions

T. Hirama, M. Takei, H. Motoyama, M. Ohta and H. Suga fabricated and measured the devices. T. Wakahara and K. Tsukagoshi analyzed the conduction properties of a C_{60} polymer system. H. Suga and K. Tsukagoshi conducted experiments and prepared the manuscript.

The manuscript was written through contributions of all authors. All authors have given approval to the final version of the manuscript.

FUNDING SOURCES

The authors would like to thank Y. Naitoh (AIST) for valuable discussions on binary switching operations. This study was supported by the JSPS KAKENHI (grant numbers 20K05291,23K17869, and 19H05460), Japan.

ACKNOWLEDGMENTS

The authors would like to thank Y. Naitoh (AIST) for the valuable discussions on binary-switching operations. This study was supported by JSPS KAKENHI (grant numbers 20K05291, 23K17869, and 19H05460), Japan. TEM observations in this study were performed under the AIRM Trial Use Program of the University of Tokyo. We thank Dr. Hiroyuki Oshikawa, Dr. Mari Morita, and Dr. Kazuhiko Moriyama for their cooperation in this study.

ABBREVIATIONS

CPTA, C_{60} pyrrolidine trisacid; STM, scanning tunneling microscopy; NDR, negative differential resistance; SEM, scanning electron microscopy; LRS, low-resistance state; HRS, high-resistance state.

FIGURE CAPTIONS

Figure 1. (a) Optical photo image with a schematic diagram of the vertical structural element, (b) Cross-sectional transmission electron microscopy (TEM) image of the vertical structural element. C_{60} pyrrolidine tris-acid (CPTA) was coated at 4000 rpm.

Figure 2. Atomic force microscopy (AFM) morphology image of the electrode surface and C_{60} pyrrolidine tris-acid (CPTA) surface spin-coated at 4000 rpm. (a) Surface of the InO_x film on the bottom electrode. (b) CPTA surface. CPTA was spin coated on the surface of InO_x (a). Scanned area of the images was 50 μm square, and the magnified area in (b) was 1 μm square. Each inset of the height profile shows surface roughness at the cutting line marked by A. Abbreviations: Average roughness (Ra) and Root mean square roughness (Rms).

Figure 3. (a) One cycle of the external voltage input sequence for the resistance switching effect in a vertically stacked structure. set voltage changes the system from the HRS to the LRS. reset voltage is for the NDR operation. Read voltage is for reading the voltages of the LRS and HRS. One cycle of the input voltage sequence was 66 sec. (b) set operation *I-V* characteristic as a function of input voltage and reset operation (c). (d) Sequential resistance changes of 100 cycles.

Figure 4. Relationship between the dose of electron beam exposure and voltage for different film thicknesses. Voltage of the negative differential resistance (NDR) transition at the reset voltage (a), and turn-on transition at the set voltage (b). The average voltages of the NDR and turn-on were evaluated for 100 cycles of *I*–*V* measurements.

Table 1. Thicknesses of the C_{60} pyrrolidine tris-acid (CPTA) films prepared by different spin-coating conditions. The thickness was measured by atomic force microscopy (AFM) at the step of the film edge.

REFERENCES

(1) Sterin, N. S.; Nivedya, T.; Mal, S. S.; Das, P. P. Understanding the Coexistence of Two Bipolar Resistive Switching Modes with Opposite Polarity in Cu_xO ($1 \leq x \leq 2$)-Based Two-Terminal Devices. *J. Mater. Sci. Mater. Electron.* **2022**, 33, 2101–2115.

(2) Zhang, H.; Yoo, S.; Menzel, S.; Funck, C.; Cüppers, F.; Wouters, D. J.; Hwang, C. S.; Waser, R.; Hoffmann-Eifert, S. Understanding the Coexistence of Two Bipolar Resistive Switching Modes with Opposite Polarity in $Pt/TiO_2/Ti/Pt$ Nanosized ReRAM Devices. *ACS Appl. Mater. Interfaces.* **2018**, 10, 29766–29778.

(3) Qian, K.; Han, X.; Li, H.; Chen, T.; Lee, P. S. Uncovering the Indium Filament Revolution in Transparent Bipolar $ITO/SiO_x/ITO$ Resistive Switching Memories. *ACS Appl. Mater. Interfaces*. **2020**, 12, 4579–4585.

(4) Yildirim, H.; Pachter, R. Mechanistic Analysis of Oxygen Vacancy-Driven Conductive Filament Formation in Resistive Random Access Memory Metal/NiO/Metal Structures. *ACS Appl. Mater. Interfaces*. **2018**, 10, 9802–9816.

(5) Ambrosi, E.; Bricalli, A.; Laudato, M.; Ielmini, D. Impact of Oxide and Electrode Materials on the Switching Characteristics of Oxide ReRAM Devices. *Faraday Discuss.* **2019**, 213, 87–98.

(6) Zhang, S.; Long, S.; Guan, W.; Liu, Q.; Wang, Q.; Liu, M. Resistive Switching Characteristics of MnO_x-Based ReRAM. *J. Phys. D: Appl. Phys.* **2009**, 42, 055112.

(7) Mehonic, A.; Munde, M. S.; Ng, W. H.; Buckwell, M.; Montesi, L.; Bosman, M.; Shluger, A. L.; Kenyon, A. J. Intrinsic Resistance Switching in Amorphous Silicon Oxide for High Performance SiOx ReRAM Devices. *Microelectron. Eng.* **2017**, 178, 98–103.

(8) Wei, Z.; Takagi, T.; Kanzawa, Y.; Katoh, Y.; Ninomiya, T.; Kawai, K.; Muraoka, S.; Mitani, S.; Katayama, K.; Fujii, S.; Miyanaga, R.; Kawashima, Y.; Mikawa, T.; Shimakawa, K.; Aono, K. Retention Model for High-Density ReRAM. *IEEE International Memory Workshop*. **2012**, 4, 1–4.

(9) Kim, K. M.; Choi, B. J.; Shin, Y. C.; Choi, S.; Hwang, C. S. Anode-Interface Localized Filamentary Mechanism in Resistive Switching of TiO_2 Thin Films. *Appl. Phys. Lett.* **2007**, *91*, 012907.

(10) Liu, Q.; Long, S.; Lv, H.; Wang, W.; Niu, J.; Huo, Z.; Chen, J.; Liu, M. Controllable Growth of Nanoscale Conductive Filaments in Solid-Electrolyte-Based ReRAM by Using a Metal Nanocrystal Covered Bottom Electrode. *ACS Nano*. **2010**, 4, 6162–6168.

(11) Sugawara, K.; Shima, H.; Takahashi, M.; Naitoh, Y.; Suga, H.; Akinaga, H. Low-Frequency-Noise Spectroscopy of TaO_x-Based Resistive Switching Memory. *Adv. Electron. Mater.* **2022**, 8, 2100758.

(12) Wu, C.-C.; Wu, W.-F.; Lin, G.-W.; Yang, W.-L. Effects of the Molecular Chain Length of Polyimide on the Characteristics of Organic Resistive Random Access Memories. *IEEE Trans. Electron Devices*. **2020**, 67, 277–282.

(13) Arunagirinathan, R. N.; Meher, N.; Iyer, P. K. Self-Assembled Naphthalimide Nanoparticles for Nonvolatile ReRAM Devices: An Efficient Approach Toward High Performance Solution-Processed and All-Organic Two-Terminal Resistive Memory Devices. *ACS Appl. Electron. Mater.* **2019**, 1, 2437–2444.

(14) Lin, W. P.; Liu, S. J.; Gong, T.; Zhao, Q.; Huang, W. Polymer Based Resistive Memory Materials and Devices. *Adv. Mater.* **2014**, *26*, 570–606.

(15) Liu, S.-H.; Yang, W.-L.; Wu, C.-C.; Chao, T.-S.; Ye, M.-R.; Su, Y.-Y.; Wang, P.-Y.; Tsai, M.-J. High-Performance Polyimide-Based ReRAM for Nonvolatile Memory Application. *IEEE Electron Dev. Lett.* **2013**, 34, 123–125.

(16) Umeta, Y.; Suga, H.; Takeuchi, M.; Zheng, S.; Wakahara, T.; Naitoh, Y.; Tsukagoshi, K. C_{60}-Nanowire Two-State Resistance Switching Based on Fullerene Polymerization/Depolymerization. *ACS Appl. Nano Mater.* **2021**, 4, 820–825.

(17) Umeta, Y.; Suga, H.; Takeuchi, M.; Zheng, S.; Wakahara, T.; Wang, Y.-C.; Naitoh, Y.; Lu, X.; Kumatani, A.; Tsukagoshi, K. Stable Resistance Switching in $Lu_3N@C_{80}$ Nanowires Promoted by the Endohedral Effect: Implications for Single-Fullerene Motion Resistance Switching. *ACS Appl. Nano Mater.* **2021**, 4, 7935–7942.

(18) Takeuchi, M.; Umeta, Y.; Suga, H.; Wakahara, T.; Wang, Y.-C.; Naitoh, Y.; Wakabayashi, K.; Tsukagoshi, K. Fullerene Nanostructure-Coated Channels Activated by Electron Beam Lithography for Resistance Switching. *ACS Appl. Nano*

Mater. **2022**, 5, 6430–6437.

(19) Takei, M.; Takeuchi, M.; Suga, H.; Wakahara, T.; Wakabayashi, K.; Okada, S.; Tsukagoshi, K. Electromechanical Switching of a C_{60} Chain in a Nanogap. *ACS Appl. Electron. Mater.* **2023**, 5, 3184–3189.

(20) Johnson, R. D.; Bethune, D. S.; Yannoni, C. S. Fullerene Structure and Dynamics: A Magnetic Resonance Potpourri. *Acc. Chem. Res.* **1992**, 25, 169–175.

(21) Stafström, S.; Fagerström, J. Electronic Structure and Stability of Fullerene Polymers. *Appl. Phys. Mater. Sci. Process.* **1997**, 64, 307–314.

(22) Yang, T.; Fukuda, R.; Cammi, R.; Ehara, M. Diels–Alder Cycloaddition of Cyclopentadiene and C_{60} at the Extreme High Pressure. *J. Phys. Chem. A*. **2017**, 121, 4363–4371.

(23) El Bakouri, O.; Garcia-Borràs, M.; Girón, R. M.; Filippone, S.; Martín, N.; Solà, M. On the Regioselectivity of the Diels–Alder Cycloaddition to C_{60} in High Spin States. *Phys. Chem. Chem. Phys.* **2018**, 20, 11577–11585.

(24) Ikuma, N.; Nakagawa, K.; Kokubo, K.; Oshima, T. Regioselective Addition of Grignard Reagents to Tosylazafulleroid and Derivatization to 1,2-Disubstituted [60]Fullerene. *Org. Biomol. Chem.* **2016**, 14, 7103–7108.

(25) Sun, B.; Ren, T.; Miao, X.; Dai, F.; Jin, L.; Yuan, H.; Xing, G.; Li, M.; Dong, J.; Chang, F.; Hu, J.; Chen, H.; Zhao, F.; Gao, X.; Zhao, Y. Isomeric and Structural Impacts on Electron Acceptability of Carbon Cages in Atom-Bridged Fullerene Dimers. *J. Phys. Chem. C*. **2008**, 112, 741–746.

(26) Bischak, C. G.; Flagg, L. Q.; Yan, K.; Li, C. Z.; Ginger, D. S. Fullerene Active Layers for N-Type Organic Electrochemical Transistors. *ACS Appl. Mater. Interfaces*. **2019**, 11, 28138–28144.

(27) Matsuo, Y. Design Concept for High-LUMO-Level Fullerene Electron-Acceptors for Organic Solar Cells. *Chem. Lett.* **2012**, 41, 754–759.

(28) Wang, Y.; Li, X.; Zhu, L.; Liu, X.; Zhang, W.; Fang, J. Efficient and Hysteresis-Free Perovskite Solar Cells Based on a Solution Processable Polar Fullerene Electron Transport Layer. *Adv. Energy Mater.* **2017**, 7, 1701144.

(29) Sun, C.; Li, X.; Wang, G.; Li, P.; Zhang, W.; Jiu, T.; Jiang, N.; Fang, J. Highly Efficient Inverted Polymer Solar Cells Using Fullerene Derivative Modified TiO_2 Nanorods as the Buffer Layer. *RSC Adv.* **2014**, 4, 19529.

(30) Vandewal, K.; Tvingstedt, K.; Gadisa, A.; Inganäs, O.; Manca, J. V. On the Origin of the Open-Circuit Voltage of Polymer–Fullerene Solar Cells. *Nat. Mater.* **2009**, 8, 904–909.

(31) Yang, Z.; Zhong, M.; Liang, Y.; Yang, L.; Liu, X.; Li, Q.; Zhang, J.; Xu, D.; SnO_2-C_{60} Pyrrolidine Tris-Acid (CPTA) as the Electron Transport Layer for Highly Efficient and Stable Planar Sn-Based Perovskite Solar Cells. *Adv. Funct. Mater.* **2019**, 29, 1903621.

(32) Huang, S.-K.; Wang, Y.-C.; Ke, W.-C.; Kao, Y.-T.; She, N.-Z.; Li, J.-X.; Luo, C.-W.; Yabushita, A.; Wang, D.-Y.; Chang, Y. J.; Tsukagoshi, K.; Chen, C.-W. Unravelling the Origin of the Photocarrier Dynamics of Fullerene-Derivative Passivation of SnO_2 Electron Transporters in Perovskite Solar Cells. *J. Mater. Chem. A*. **2020**, 8, 23607–23616.

(33) Xue, D.; Wakahara, T.; Marumoto, K.; Tsukagoshi, K. High Charge Transfer from C_{60} Pyrrolidine Tris-Acid to SnO_2 Electron Transport Layer Directly Observed by ESR Spectroscopy. *ACS Appl. Energy Mater.* **2023**, *6* , 2434–2439.

(34) Onoe, J.; Nakayama, T.; Aono, M.; Hara, T. Structural and Electrical Properties of an Electron-Beam-Irradiated C_{60} Film. *Appl. Phys. Lett.* **2003**, 82, 595–597.

(35) Masuda, H.; Onoe, J.; Yasuda, H. High-Resolution Transmission Electron Microscopic and Electron Diffraction Studies of C_{60} Single Crystal Films before and after Electron-Beam Irradiation. *Carbon*. **2015**, 81, 842–846.

(36) Onoe, J.; Nakayama, T.; Aono, M.; Hara, T. The Electron Transport Properties of Photo- and Electron-Beam-Irradiated C_{60} Films. *J. Phys. Chem. Solids*. **2004**, 65, 343–348.

(37) Onoe, J.; Ochiai, Y.; Ito, T.; Kimura, S.; Ueda, S.; Noguchi, Y.; Ohno, K. Electronic and Electron-Transport Properties of Peanut-Shaped C_{60} Polymers. *J. Phys. Conf. Ser.* **2007**, 61, 899–903.

(38) Nakaya, M.; Aono, M.; Nakayama, T. Scanning Tunneling Microscopy and

Spectroscopy of Electron-Irradiated Thin Films of C_{60} Molecules. *Carbon*. **2011**, 49, 1829–1833.

(39) Larson, B. W.; Whitaker, J. B.; Popov, A. A.; Kopidakis, N.; Rumbles, G.; Boltalina, O. V.; Strauss, S. H. Thermal [6,6] → [6,6] Isomerization and Decomposition of PCBM (Phenyl-C_{61} -Butyric Acid Methyl Ester). *Chem. Mater.* **2014**, *26* , 2361–2367.

(40) Regulska, E.; Breczko, J.; Rodziewicz, P. Solvent Effect on C_{60} Tris-Acid Solubility: Light Scattering, Spectroscopic, Electrochemical and Computational Studies. *Diam. Relat. Mater.* **2021**, 116, 108427.

TOC

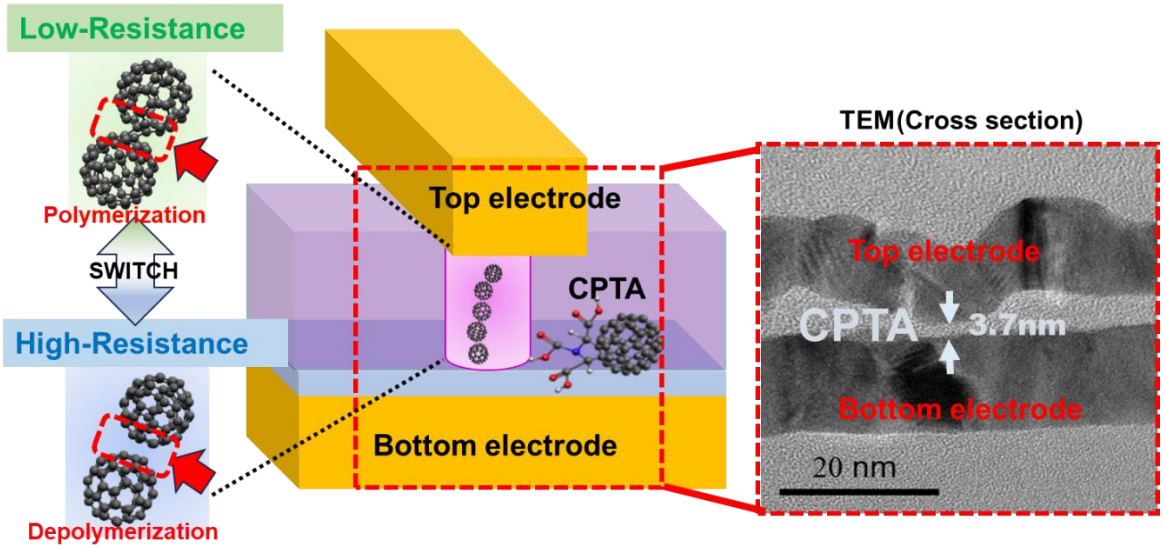
Low-Resistance
Polymerization
SWITCH
High-Resistance
Depolymerization
Top electrode
CPTA
Bottom electrode
TEM(Cross section)
Top electrode
CPTA
3.7nm
Bottom electrode
20 nm